Organic Geochemistry 175 (2023) 104507

Contents lists available at ScienceDirect

Organic Geochemistry

journal homepage: www.elsevier.com/locate/orggeochem

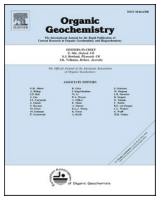

A maturation scale for molecular simulation of kerogen thermal degradation

Qiuya Han [a], Meijun Li [a,b,*], Xiaoqiang Liu [c], Hong Xiao [a], Junhao Ren [a], Chengbo Guo [a]

[a] State Key Laboratory of Petroleum Resources and Prospecting, College of Geosciences, China University of Petroleum, Beijing 102249, China
[b] Key Laboratory of Exploration Technologies for Oil and Gas Resources, Ministry of Education, College of Resources and Environment, Yangtze University, Wuhan 430100, China
[c] College of Chemistry and Environmental Engineering, Sichuan University of Science and Engineering, Zigong 643000, China

ARTICLE INFO

Associate Editor — Joseph Curiale

Keywords:
Kerogen
Maturity
ReaxFF molecular dynamics simulation
Vitrinite reflectance

ABSTRACT

Correlating molecular dynamics (MD) simulations of thermal degradation of organic matter with natural processes in ancient sediments is vital for revealing the mechanisms of hydrocarbon generation at molecular and atomic levels. This study establishes a practical maturation scale for molecular modeling of the thermal degradation of kerogen. ReaxFF reactive MD simulations of the thermal evolution of typical kerogen types (Type I, II, and III) were carried out at temperatures ranging from 1200 K to 2600 K. The results demonstrate that the H/C and O/C atomic ratios of kerogen molecules decrease as simulation temperatures increase and that the evolutionary paths of the three kerogen types fit well with those shown in the van Krevelen diagram. The corrected activation energies of pyrolysis for these three typical kerogen types were found to be 61.1 kcal/mol, 53.5 kcal/mol and 52.8 kcal/mol, respectively, consistent with those obtained from both laboratory simulations and basin modeling. By comparison with the relationships between measured vitrinite reflectance values and the H/C atomic ratios of kerogen samples reported in the literature, a quantitative relationship was established between the vitrinite reflectance (%Ro) values of kerogen and simulation temperatures (T). The cross-plots of T vs %Ro for kerogen types II and III show that vitrinite reflectance exponentially increases with increasing simulation temperature. Two logarithmic correlation equations were constructed to match geological maturation levels to the corresponding levels in MD simulations of thermal degradation of types II and III kerogen. These maturation scales are generally in line with the simulation temperatures set for thermal degradation in kerogen pyrolysis in previous studies. This work has promising practical implications for research on the thermal evolution behavior of ancient sedimentary organic matter using ReaxFF MD simulation.

1. Introduction

Kerogen is the predominant form of dispersed insoluble organic matter (OM) in sedimentary rocks and is of great importance as the source of petroleum (Durand, 1980; Tissot and Welte, 1984; Hunt, 1996; Vandenbroucke and Largeau, 2007). Kerogen also carries valuable information relating to paleoenvironmental evolution, paleoclimate, and the biotas of the Earth (Vandenbroucke and Largeau, 2007). Numerous studies have been carried out on the isolation, classification, biological sources, compositions, chemical structures, natural evolution, and laboratory simulation of kerogen, as well as various analytical techniques (e.g., Tissot and Welte, 1984; Vandenbroucke and Largeau, 2007). The abundance, type, and maturation of kerogen are three of the main factors used for source rock assessment in petroleum geology and geochemistry (Tissot and Welte, 1984; Hunt, 1996). In particular, determining the thermal maturity of kerogen is essential for predicting the quality and quantity of hydrocarbons generated in a given source rock kitchen.

Various scales, based on chemical and physical (including optical) properties, such as vitrinite reflectance (%Ro), H/C and O/C atomic ratios are widely applied to determine the maturation levels of kerogen. For example, atomic H/C ratios of kerogen are excellent indicators of thermal maturity for end-member kerogen types (Baskin, 1997). Due to its wide use, the vitrinite reflectance scale has also long been considered

* Corresponding author at: State Key Laboratory of Petroleum Resources and Prospecting, College of Geosciences, China University of Petroleum, Beijing 102249, China.
E-mail address: meijunli@cup.edu.cn (M. Li).

https://doi.org/10.1016/j.orggeochem.2022.104507
Received 26 July 2022; Received in revised form 6 October 2022; Accepted 7 October 2022
Available online 20 October 2022

as a reliable reference. For instance, Burnham and Sweeney (1989) presented an equation for H/C atomic ratio and vitrinite reflectance based on a chemical kinetic model. Buchardt and Lewan (1990) investigated naturally matured Early Paleozoic Alum shale in hydrous pyrolysis laboratory experiments and found that there is an excellent negative correlation between the reflectance values of vitrinite-like macerals and the atomic H/C ratios of isolated kerogen. This %Ro vs H/C atomic ratio correlation compares well with that of Devonian-Mississippian black shale (Lewan, 1987).

Smith and Smith (2007) determined an empirical relationship between the carbon and hydrogen contents of coals and their measured vitrinite reflectance by analyzing more than 200 samples from 60 coal seams. More recently, Craddock et al. (2020) reported that the chemical and physical properties of Type II kerogen are dependent on thermal maturation. They obtained a universal curve relating Type II kerogen properties (e.g., the molar H/C ratio of kerogen) to thermal maturity (i.e., vitrinite reflectance) based on analysis of Type II kerogen from 15 petroleum-bearing formations around the world.

Numerical simulation is a practical method for investigating the thermal maturation behavior of kerogen based on temperature–time compensation principles (Tissot and Welte, 1984). The thermal evolution paths and chemical features of kerogen and related products in simulations are comparable with those found in sedimentary basins. Sweeney and Burnham (1990) developed a simplified EASY%Ro model using an Arrhenius first-order parallel-reaction approach, which is applicable for heating rates ranging from those applied in the laboratory to those that occur naturally in slowly subsiding geological settings. The EASY%Ro method therefore provides a practical maturation scale that can be used to directly relate laboratory simulations to geological data. Another model developed by Tang et al. (1996) provides an improved understanding of early methane generation in coal, based on anhydrous, sealed-tube pyrolysis experiments and extrapolation of kinetic parameters.

Traditional laboratory tests and experiments are considered to be the most reliable methods for characterizing the thermal evolution processes and hydrocarbon generation mechanisms of kerogen. The disadvantage is that laboratory analysis is costly and time-consuming. The detailed reactions are also difficult to understand from laboratory experiments due to the lack of effective methods for detecting intermediates. Molecular dynamic (MD) simulation is recognized as an effective alternative method for investigating complex systems at the atomic and molecular levels (Leach, 2021). MD has been applied widely in biology, materials science, chemistry, pharmacy, and other disciplines (Leach, 2021). It has also attracted considerable attention in organic geochemistry, and consequently in petroleum exploration and development (Seyyedattar et al., 2019; Li et al., 2021).

In the past two decades, van Duin et al. (2001), Chenoweth et al. (2008) and Castro-Marcano and van Duin (2013) have developed a reactive force field (ReaxFF) that can be used for molecular dynamic simulation of large scale reactive chemical systems. ReaxFF MD provides a practical tool for simulating the evolution and transformation of complex macromolecular organic matter. A great deal of reactive MD simulation work using ReaxFF has been done on the thermal evolution of coal (Salmon et al., 2009; Zhang and LeBoeuf, 2009; Zheng et al., 2014; Hong and Guo, 2017; Xu et al., 2019; Zhang et al., 2020). Several attempts have also been made to investigate chemical mechanisms and product distributions in the thermal evolution of kerogen using ReaxFF MD simulation (Liu et al., 2015; Qian et al., 2016; Pawar et al., 2017; Zhang et al., 2021). In these studies, different reaction temperatures were used to reveal the characteristics of the reaction system at various stage of geological thermal evolution. The results show that the kerogen pyrolysis via ReaxFF MD method probably begins at a temperature of approximately 1300 K on the molecular dynamics scale (Liu et al., 2015; Pawar et al., 2017). Liu et al. (2015) modeled product distribution and residual kerogen fragments in NVT (constant volume and constant temperature) simulations at temperatures of 1800 K, 2000 K, 2200 K, and 2400 K. However, in the absence of a numerical scale to correlate maturation levels of kerogen in MD simulations to geological maturity, it has not yet been possible to obtain a full understanding of the mechanisms and processes of natural thermal evolution using MD.

Here we study the H/C and O/C atomic ratios in typical type I, II and III kerogen molecules (Kelemen et al., 2007; Ungerer et al., 2015) under different simulation temperatures using ReaxFF reactive MD simulation. A primary maturation scale for ReaxFF MD can be established by comparison with the published relationships between H/C atomic ratios and measured vitrinite reflectance values of kerogen samples. The activation energy of pyrolysis of kerogens was also calculated to test the rationality of the simulation. The results have potential practical implications for research on thermal evolution features of organic matter in ReaxFF reactive MD simulations.

2. Materials and methods

2.1. Kerogen molecular models

Three kerogen molecular models, as proposed by Ungerer et al. (2015), were used in this study to represent typical kerogen macromolecules for MD simulation (Fig. 1). The Type I model represents the molecular structure of hydrogen-rich kerogen deposited in an anoxic lacustrine environment, such as the Eocene Green River oil shale in Colorado. The model contains 251 carbon atoms, and its chemical formula is $C_{251}H_{385}O_{13}N_7S_3$. The Type II model was built to represent oil-prone organic matter deposited in an anoxic marine environment. It has a chemical formula of C_{252} $H_{294}O_{24}N_6S_3$. The Type III model is representative of typical organic matter originating from higher plants, which is characterized by more oxygen and fewer hydrogen atoms than Type I and Type II kerogen. Its chemical formula is $C_{233}H_{204}O_{27}N_4$.

The chemical properties and structures of these three kerogen molecular models are consistent with experimental results from analysis of natural geological samples (including elemental analysis, ^{13}C NMR and X-ray photoelectron spectroscopy). The structural characteristics of each type of kerogen molecular model (element composition, aromatic carbon content, functional group species, side chain length, and so on) are described at length in Section 3.1.

In brief, the types I, II and III kerogen models established by Ungerer et al. (2015) are considered to be satisfactory representations of typical organic matter types in the immature thermal stage. They have been employed successfully in MD simulations in previous studies; for example, in analyzing the competitive adsorption behavior of CH_4 and CO_2 on kerogen surfaces (Huang et al., 2018), supercritical methane diffusion in shale nanopores (Wang et al., 2018), and the adsorption behavior of shale oil in kerogen (Yang et al., 2020).

2.2. Molecular dynamics simulation details

The three kerogen molecular models were incorporated into cubic cells using the Amorphous Cell code in Materials Studio (Accelrys, 2013), with a low bulk density of 0.30 g/cm^3. In order to obtain reliable densities, a series of MD simulations were performed using the Forcite software package, adopting the simulation methods used by Liu et al. (2020). The simulation results indicated bulk densities of types I, II and III kerogens of 0.999, 1.018 and 1.180 g/cm^3, respectively. This is in good agreement with experimental data (Ungerer et al., 2015). The final parameters of the primitive cells for the three types of kerogens were $a = 23.26$ Å, $b = 34.44$ Å, $c = 17.95$ Å, $\alpha = 47.93$ degree, $\beta = 38.58$ degree, $\gamma = 68.34$ degree for the Type I kerogen cell; $a = 22.90$ Å, $b = 31.29$ Å, $c = 25.32$ Å, $\alpha = 103.98$ degree, $\beta = 136.83$ degree, $\gamma = 113.72$ degree for the Type II kerogen cell; $a = 14.39$ Å, $b = 22.07$ Å, $c = 30.95$ Å, $\alpha = 105.03$ degree, $\beta = 119.44$ degree, $\gamma = 35.94$ degree for the Type III kerogen cell. As shown in Fig. 2, pyrolysis models of the three types of kerogen cells were determined using a $2 \times 2 \times 2$ supercell along x, y and z directions, containing 5272 atoms ($C_{2008}H_{3080}N_{56}O_{104}S_{24}$) for the

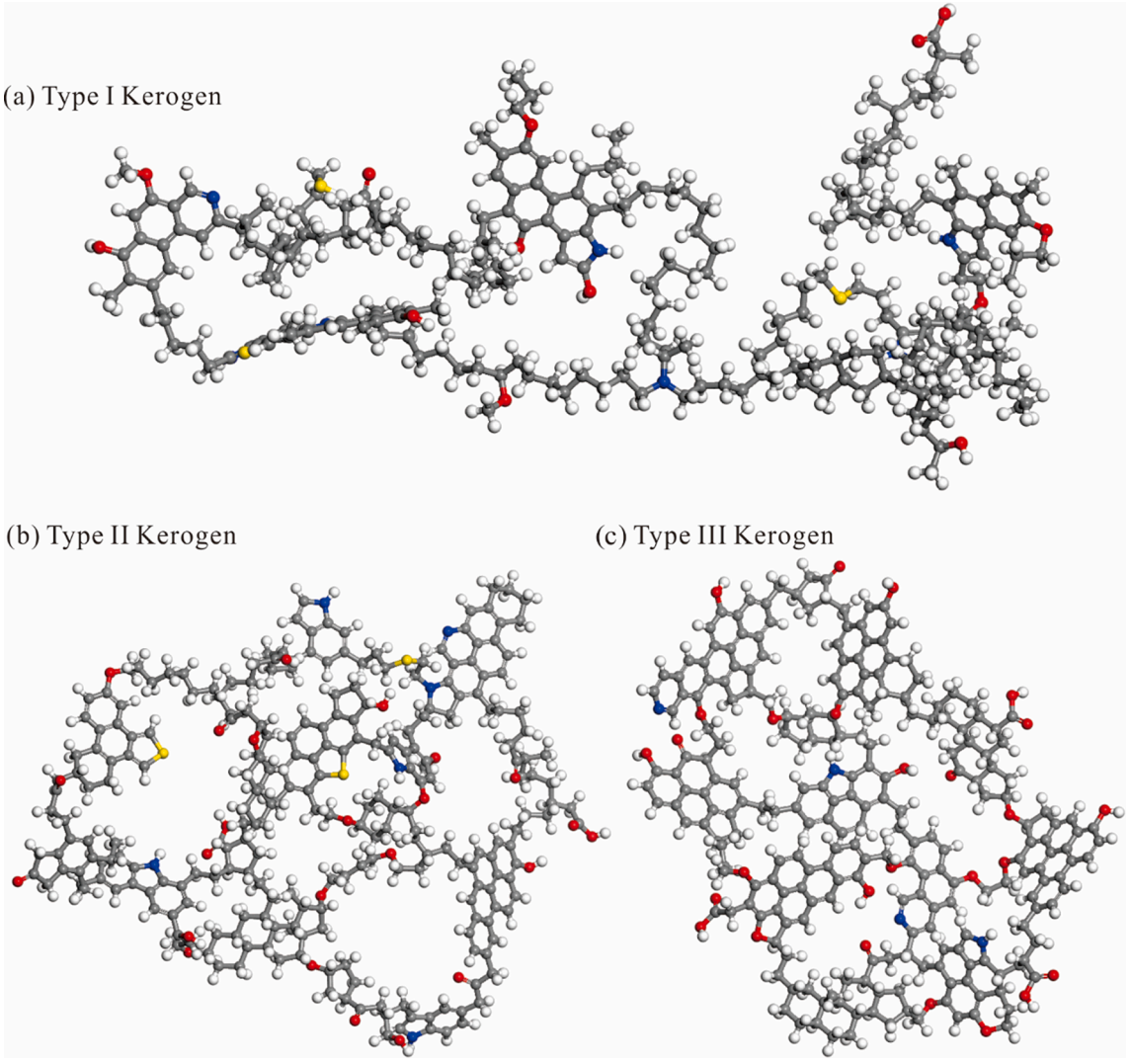

Fig. 1. Chemical structures of models of three typical types of kerogen, as proposed by Ungerer et al. (2015).

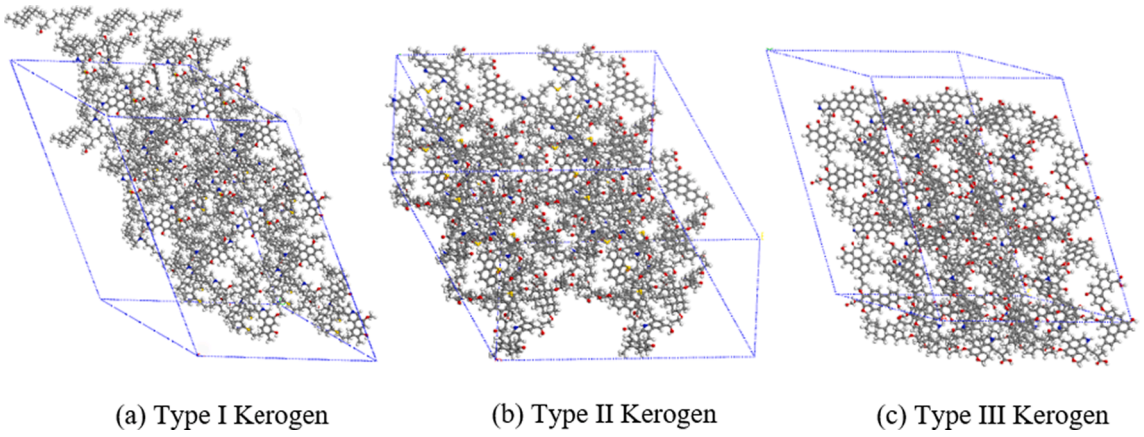

Fig. 2. Pyrolysis models of three types of kerogen cells.

Type I kerogen cell, 4632 atoms ($C_{2016}H_{2352}N_{48}O_{192}S_{24}$) for the Type II kerogen cell and 3744 atoms ($C_{1864}H_{1632}N_{32}O_{216}$) for the Type III kerogen cell. Final supercells for the three types of kerogen cells were then used to simulate pyrolysis by performing ReaxFF reactive molecular dynamics simulations.

ReaxFF reactive force fields (van Duin et al., 2001; Chenoweth et al., 2008) have been applied widely to obtain insights into the mechanisms of thermal pyrolysis of various hydrocarbon fuels, as they can predict the breaking and forming of bonds during thermal simulations. All the MD simulations in this study were performed using LAMMPS code (Aktulga

et al., 2012) with ReaxFF reactive force fields. The potentials parametrized for the CHONS system were adopted from the work of Zhang et al. (2021). To reveal the reaction mechanisms of kerogen pyrolysis, a range of ReaxFF MD simulations, with constant temperature and volume ensemble (NVT), were performed. The two key parameters of pressure and temperature were controlled using a Nose–Hoover barostat and thermostat (Shinoda et al., 2004). NVT MD simulations were then performed in the temperature range of 1200– 2600 K, at ten temperatures (1200, 1400, 1500, 1600, 1800, 2000, 2200, 2400, 2500, and 2600 K). A time step of 0.1 fs, a bond cutoff value of 0.5 Å, a total simulation time of 500 ps, and a heating rate of 10 K/ps were set during all NVT-ReaxFF MD simulations. The early decay of kerogen and subsequent formation of smaller molecules were described by a series of FORTRAN scripts (Xue et al., 2017).

It is worth noting that the time scales of high-temperature ReaxFF MD simulations are much shorter than the slow thermochemical transformation of kerogen that occurs during catagenesis on geological time scales (several to tens of millions of years). More recently, compared to conventional MD, Atmani et al. (2017, 2020) reported an advanced method — the replica exchange molecular dynamics (REMD) method that applies reactive molecular dynamics within an accelerated simulation framework, and can perform RMD simulations at lower temperature, close to geological conditions (150 °C and 10–100 MPa). Valdenaire et al. (2020) proposed an accelerated method based on flux sampling and kinetic integration along a 1D order parameter that can considerably extend the accessible time scales. However, due to the considerable impact of these methods on the cost of computation, the pyrolysis simulations in this study were run at higher temperatures which allowed the chemical reactions to occur within extremely short periods of time (So Rensen and Voter, 2000; Paajanen and Vaari, 2017). This is a commonly accepted approach to simulating pyrolysis using ReaxFF MD (Liu et al., 2015). Pawar et al. (2017) also confirmed that ReaxFF MD simulations at high temperatures and on very short time scales can provide valuable insights into the processes that occur in sedimentary basins on geological time scales, in much the same way that has been used to obtain information regarding kerogen maturation in pyrolysis and flash pyrolysis (Burnham and Happe, 1984; Sinninghe Damsté et al., 1989).

2.3. Determination of kerogen H/C and O/C atomic ratios at different temperatures

The ReaxFF MD approach reveals modeled elemental compositions and chemical structures of residual kerogen molecular fragments in the thermal evolution process, providing a valuable complement to traditional laboratory simulations. Variations in the H/C and O/C atomic ratios of residual kerogen have been commonly used in previous geological studies and laboratory pyrolysis experiments as parameters for distinguishing thermal maturation stages.

The principles and methods for calculating the H/C and O/C atomic ratios of residual kerogen molecular fragments after pyrolysis at different simulation temperatures are as follows: (1) The simulation products are classified according to the number of carbon atoms. C_1–C_4 fragments are considered as gas; C_5–C_{13} and C_{14}–C_{40} fractions are considered as tar; and C_{40+} fragments are considered as char. This classification is based on molecular weights of experimental data (Fletcher et al., 1992) as well as shown in the simulation literature (Zheng et al., 2014; Qian et al., 2016). C_{40} was chosen as the cutoff on the understanding that C_{40+} molecular fragments can be treated as residual kerogen. The average values of the H/C and O/C ratios for all C_{40+} macromolecules are therefore used to represent the ratios of kerogen at specific simulation temperatures. (2) During pyrolysis, no residual C_{40+} of high-molecular-weight structures was observed at higher temperatures because C_{40+} compounds gradually decompose into smaller molecules with increasing temperature. However, it was observed that the molecular structures of C_{17}–C_{40} products also had similar characteristics to those of the kerogen molecules. In this instance, fragments with carbon numbers from 17 to 40 were accordingly defined as residual kerogen. (3) Theoretically, the H/C and O/C atomic ratios of kerogen should gradually decrease with increasing thermal maturation levels. Fragments at a given temperature with H/C ratios higher than those in relatively lower temperatures were eliminated to avoid the possible incorporation of products of kerogen degradation. It should be noted that, while the absolute size of the kerogen fragments in the MD simulations with C_{17} to C_{40+} may not exactly match those of kerogens in actual geological conditions, the H/C and O/C ratios of the MD kerogens match those of geological kerogen.

3. Results

3.1. The molecular models of the three kerogen types

As mentioned in Section 2.1, the molecular models of the three kerogen types proposed by Ungerer et al. (2015) were used in the simulation. Detailed elemental compositions, aromatic carbon content, and functional group species of the three kerogen molecules were derived as follows.

The H/C and O/C atomic ratios of the Type I kerogen molecule are 1.53 and 0.051, respectively. The distribution of carbon numbers is dominated by non-aromatic carbon with long linear or branched chains, and the aromaticity is relatively low. The oxygen atoms in the Type I model occur in ether bridges, hydroxyl groups (mainly phenolic), carbonyl groups, and carboxylic groups with relatively low abundance. There are, in total, seven nitrogen atoms and three sulfur atoms in this molecular model, which are involved in the nitrogen-containing (pyrrolic groups, pyridinic group, and quaternary nitrogen) and sulfur-containing (sulfide bridge, thiol group, and thiophenic structures) functional groups.

The Type II kerogen model contains 252 carbon atoms, 294 hydrogen atoms, and 24 oxygen atoms. The H/C and O/C atomic ratios are 1.17 and 0.097, respectively. Aromaticity is 40%, and the average number of carbon atoms per aromatic cluster is 12. Polycyclic saturated structures, such as the backbones of steranes and hopanes, occur in the Type II kerogen model but not the Type I kerogen model. The contents and distributions of nitrogen and sulfur atoms in the model are similar to those in the Type I kerogen model.

The oxygen content of the Type III kerogen molecular model ($C_{233}H_{204}O_{27}N_4$) is significantly higher. The H/C and O/C atomic ratios are 0.87 and 0.11, respectively. Average aromaticity is as high as 52%, and the average size of the aromatic units is also larger than those in the Type I and II kerogen models.

All the kerogen molecular models were geometrically optimized, and the final structures are substantially more folded, stable, and compact than the initial configurations. These optimized structures are reliable for subsequent molecular dynamics (MD) simulation calculations.

3.2. H/C and O/C atomic ratios of kerogen at different simulation temperatures

Analysis was conducted to determine the variations in the H/C and O/C ratios of the three kerogen types at room temperature (T = 298 K) and at simulation temperatures across the range 1200–2600 K (Fig. 3). The H/C atomic ratio of Type I kerogen decreases smoothly from 1.53 at 298 K to 1.48 at 1800 K, indicating that only minor hydrogen loss occurs, and that no significant petroleum is generated. When the simulation temperature is increased to 1800 K, the H/C ratio begins to decrease sharply, which is likely to represent the onset of the principal oil formation zone in Type I kerogen.

Variations in H/C atomic ratios with simulation temperature for types II and III kerogen resemble those of Type I kerogen. The most notable difference is that the sharp decline in H/C atomic ratios for both Type II and III kerogen begin at about 1600 K. This indicates that their

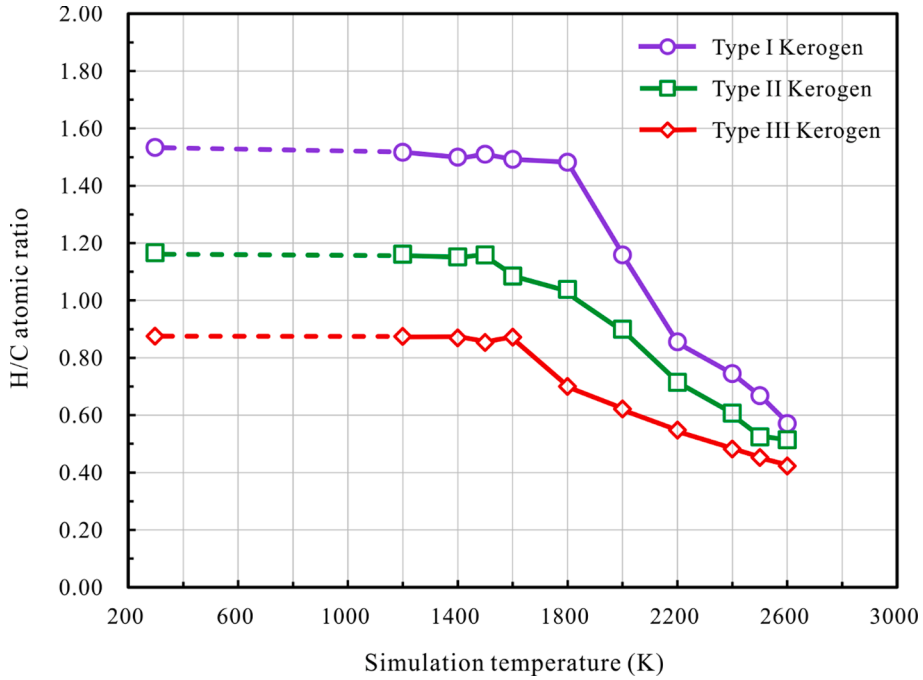

Fig. 3. Variations in H/C atomic ratios with increasing simulation temperature for three typical types of kerogen.

thresholds for significant hydrocarbon generation are lower than that of Type I kerogen, which is consistent with natural thermal evolution (Vandenbroucke and Largeau, 2007). In addition, their rates of decline during the 1800–2200 K stage are lower than that of Type I kerogen (Fig. 3).

The O/C ratio of Type I kerogen shows the lowest initial value (0.052), with only relatively small changes between 298 K and 2600 K (Fig. 4). The initial O/C ratio of Type II kerogen (0.095) is markedly higher than that of Type I kerogen. However, by the time the simulation temperature reaches 1200 K, the O/C ratio of Type II kerogen has decreased to 0.070. The ratio decreases continuously with increase in the simulation temperature, reaching its lowest value (0.025) at 2600 K. Type III kerogen has the highest initial O/C ratio value (0.116), and its rate of decline may be lower than that of Type II kerogen between 298 K and 1200 K (Fig. 4). When the simulation temperature exceeds 1200 K, the O/C ratio begins to decrease rapidly, with slight fluctuations, reaching its lowest value (0.034) at 2600 K. This may be due to preferential elimination of hydrogen and carbon, and the O/C ratio may even increase according to variations in the relative concentrations of these elements. Another possible explanation is the limited number of oxygen atoms in the kerogen molecular model. As shown in Fig. 3, the O/C ratios for the three types of kerogen are approximately consistent at

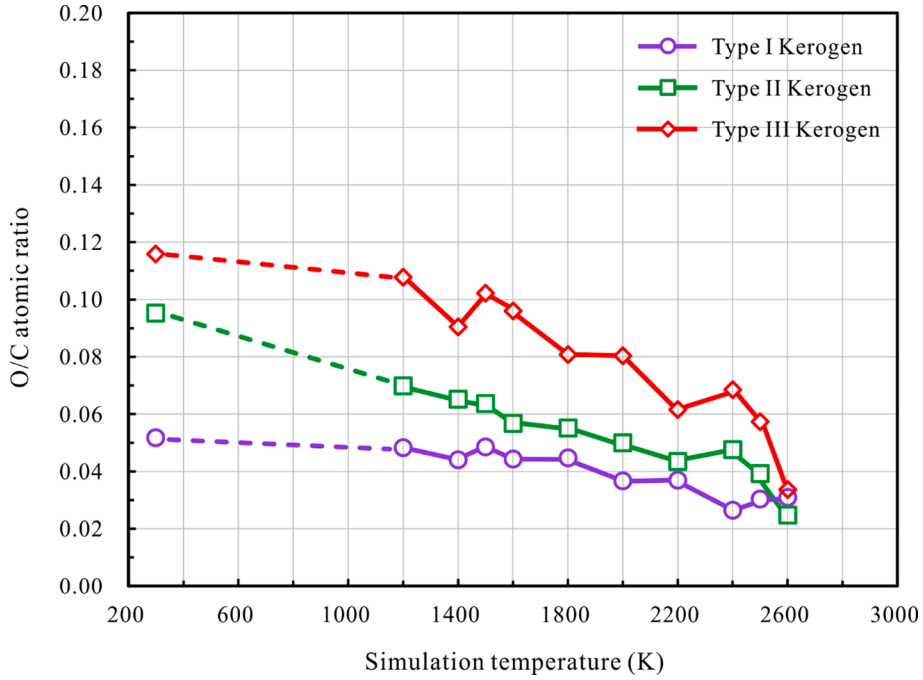

Fig. 4. Variations in O/C atomic ratios with increasing simulation temperature for three typical types of kerogen.

2600 K (Fig. 4), which occurs earlier than the H/C ratios.

3.3. Kinetic analysis of the pyrolysis of kerogen

Pyrolysis simulation of the three kerogen types at different temperatures and kinetic analysis of kerogen pyrolysis by calculating reaction rates, can be used to derive kinetic data from weight loss reactions of kerogen. Here, we substitute the mass fraction of the original compound for concentration, following the detailed calculation method set out by Zhang et al. (2020). The degree of conversion is determined by formula 1 under the assumption that kerogen pyrolysis is a first-order reaction. The rate constant k of the reaction conforms to the Arrhenius equation. According to the first-order reaction kinetic model, activation energy can be described by equations (2) and (3).

$$\alpha = \left(w_{t,0} - w_t\right)/w_{t,0} \quad (1)$$

$$d\alpha/d\tau = k(1-\alpha) \quad (2)$$

$$k = A\exp(-E_a/RT) \quad (3)$$

where w_t is the weight of non-volatile products after pyrolysis, $w_{t,0}$ is the initial weight of the kerogen model, α is the degree of conversion within τ time, E_a is the activation energy of the thermostatic weightlessness reaction, A is the pre-exponential factor, and k is the weight loss rate constant.

Fig. 5 shows the Arrhenius plots of ln k vs $1000/T$ for kerogen pyrolysis at 1200–2600 K. It can be seen that all of the Arrhenius plots have good linearity. The rate constant of the weightlessness reaction increases with increase in temperature. According to the fitting sum, the activation energies (E_a) for the three typical kerogen types were determined as 73.9 kcal/mol, 59.7 kcal/mol, and 60.2 kcal/mol, respectively. In addition, the standard errors of the slopes of the regression equations were calculated for linear fit, and were 1.54, 0.75 and 0.89 for Type I, II and III kerogens, respectively. The slope of the regression equation of the fitting curve was corrected by standard error, and the activation energies of the three types of kerogen after correction were 61.1 kcal/mol, 53.5 kcal/mol, 52.8 kcal/mol, respectively, which are basically consistent with the values obtained from both laboratory simulation and basin modeling. Although the distribution of activation energies obtained by analyzing data from pyrolysis experiments is typically quite broad when the kinetics are represented by a set of parallel reactions, it is typically dominated by activation energies in the 45–70 kcal/mol range (Ungerer et al., 1990; Pepper and Corvit, 1995; Behar et al., 1997; Burnham, 2015). When the three types of kerogen were regressed together, the calculated activation energy was 64.6 kcal/mol and the correlation coefficient (r^2) of the regression equation was 0.86. For separate regressions, the correlation coefficients corresponding to the three fitting curves are 0.85, 0.94 and 0.92, respectively. The fitting effect of separate regressions is better than that of a single regression. It is, therefore, preferable that the activation energies of the three types of kerogen are regressed separately.

4. Discussion

4.1. van Krevelen diagram

The van Krevelen diagram was first proposed in 1961 (van Krevelen, 1961), and since then has played an important role in the identification of kerogen types and in the development of concepts and understandings regarding the evolutionary paths of coals and kerogens. The diagrams can be used to trace the diagenetic, catagenetic, and metagenetic stages of geological samples (Fig. 6) (van Krevelen, 1961).

Depending on the biological source materials, three principal types of kerogen (I, II and III) are conventionally distinguished. Fig. 6 shows that, in this study, the evolutionary paths of the three types of kerogen, based on molecular simulation, are consistent with the typical models proposed by van Krevelen (1961). From the diagenesis stage to the early period of the catagenetic stage (< 0.7 %Ro and ~1600 K in this study), the hydrogen element contents of the three types of kerogen decrease slowly while the oxygen element contents decrease rapidly. This is evident in Fig. 6 as a rapid decrease in the O/C ratio accompanied by only a minor change in the H/C ratio. The catagenesis stage (~0.7 < %Ro < ~2.0 and ~1600–2500 K in the study) is characterized by a rapid decrease in the H/C ratio (Fig. 6), which corresponds to the main hydrocarbon generation stage. The H/C ratios of types I, II, and III kerogen decreased from 1.49, 1.09, 0.87 to ~0.50, respectively. During the early metagenesis stage (%Ro > ~2.0 and > 2500 K in the study), the H/C and O/C ratios of the three types of kerogen decreased to their lowest levels (~0.40 and ~ 0.30, respectively), and all the kerogen types tended to have similar elemental compositions (Fig. 6).

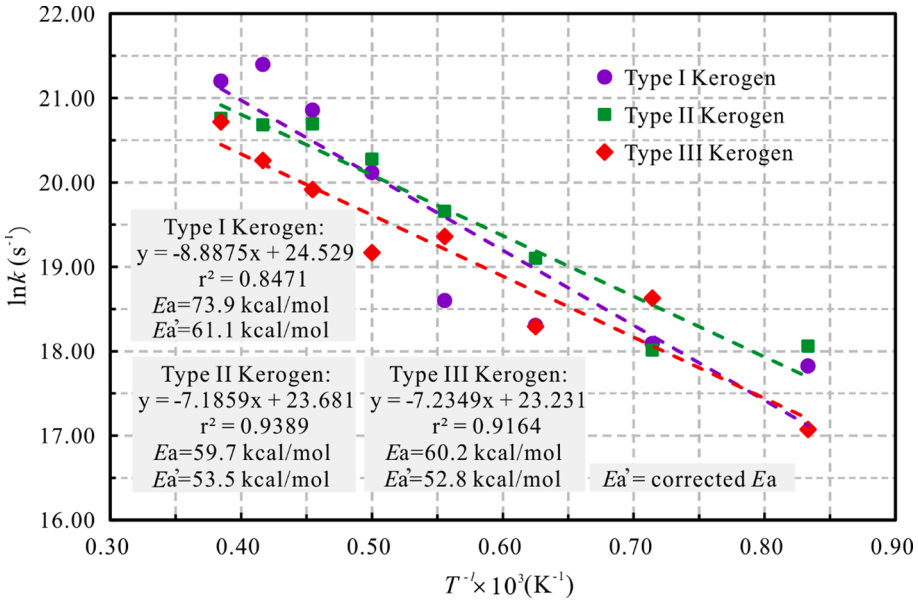

Fig. 5. Weight loss rate constant for three typical types of kerogen pyrolysis based on ReaxFF results.

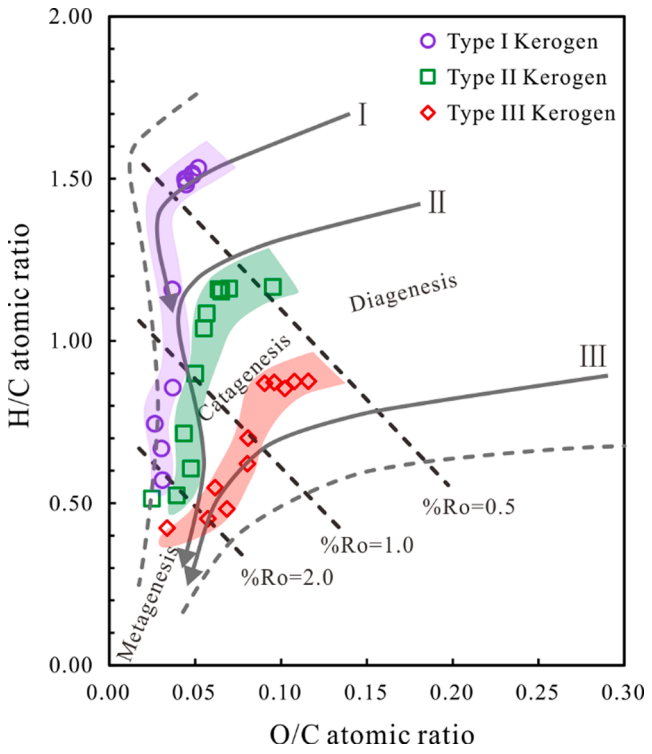

Fig. 6. H/C and O/C atomic ratios of kerogen molecules at different simulation temperatures in the van Krevelen diagram (after Tissot and Welte, 1984).

4.2. Relationship between the H/C atomic ratio and vitrinite reflectance %Ro

To a certain extent, the elemental composition of kerogen determines its basic structure. For example, a molecule with C:H = 1:4 is methane, and groups in kerogen with C:H = 1:2 exist as saturated structures. Therefore, the ratio of hydrogen to carbon atoms in kerogen can reflect its chemical structure (Baskin, 1997). The H/C atomic ratios of kerogen have therefore been correlated with the extent of thermal conversion of organic matter (Baskin, 1997). Vitrinite reflectance is the most widely applied thermal maturity indicator in petroleum exploration (Hunt, 1996). Numerous studies have been carried out to precisely determine the relationship between vitrinite reflectance (in units of %Ro) and the H/C atomic ratio (e.g., Burnham and Sweeney, 1989; Sweeney and Burnham, 1990; Buchardt and Lewan, 1990; George et al., 1994; Smith and Smith, 2007; Bandopadhyay and Mohanty, 2014; Burnham, 2019; Craddock et al., 2020; Lohr and Hackley, 2021).

George et al. (1994) reported that vitrinite reflectance (as %Ro) is related to the H/C atomic ratio in Type III kerogen, based on their analysis of coal samples from the Permian Greta seam in the Sydney basin. They expressed this relationship as follows (equation (4)):

$$\%Ro = 2.12 - 1.71(H/C) \quad (4)$$

Smith and Smith (2007) analyzed 210 Australian coal samples and proposed equation (5), which links vitrinite reflectance (%Ro) to the element ratio. The slope of this equation is steeper than that of equation (4).

$$\%Ro = 3.06 - 2.93(H/C) \quad (5)$$

Interestingly, Smith and Smith (2007) found that the increase in slope with decreasing H/C atomic ratio fits slightly better with an exponential function than with a linear fit. As a result, equation (6) was set up for exponential fit.

$$\%Ro = 6.86\exp[-2.83(H/C)] \quad (6)$$

Burnham and Sweeney (1989) established a model relating %Ro to elemental composition based on numerical simulation and derived the relationship described in equation (7) by inspection.

$$\%Ro = 12\exp[-3.3(H/C)] - (O/C) \quad (7)$$

For Type II kerogen, Buchardt and Lewan (1990) constructed a relationship (equation (8)) between the reflectance values of vitrinite-like macerals and the atomic H/C ratios of isolated kerogen from Alum shale through hydrous pyrolysis simulation experiments. It was also found that the %Ro vs H/C correlation (equation (9)) for Devonian-Mississippian black shale generally coincided with equation (8) (Lewan, 1987).

$$\log(\%Ro) = -1.018(H/C) + 0.812 \quad (8)$$

$$\log(\%Ro) = -1.044(H/C) + 0.816 \quad (9)$$

More recently, Craddock et al. (2020) summarized previous published data from petroliferous sedimentary basins with different ages and formations. They found that the molar H/C ratio of Type II kerogen presents a single maturity trend with thermal maturity expressed as vitrinite reflectance (%Ro). However, no specific quantitative relationship was given in that study, so 73 data points were extracted from Fig. 2 in Craddock et al. (2020) using graph digitizer software, and the data were used to fit equation (10).

$$\%Ro = \exp\{[0.8225 - (H/C)]/0.418\} \quad (10)$$

Due to the absence of vitrinite macerals in Type I kerogen, the utility of vitrinite reflectance as a maturity indicator is limited (Alpern, 1980). However, until now, no reasonable and practical alternative formula for Type I kerogen has been proposed.

4.3. The maturity scale for molecular simulation of kerogen

Based on the quantitative relationships between %Ro and H/C set out in the previous equations, a maturity scale for molecular simulation of kerogen thermal degradation can be established. The equivalent vitrinite reflectance for molecular simulation at different temperatures can then be determined.

Considering the significant differences in calculated %Ro between different kerogen types for each equation, the relationship %Ro vs T needs to be determined for types II and III kerogen, respectively.

For Type II kerogen, the %Ro vs H/C equations (8) and (9) proposed by Buchardt and Lewan (1990) and Lewan (1987) are generally consistent, and are also similar to the %Ro vs H/C relationship determined by Craddock et al. (2020). Taking into account the comprehensiveness and diversity of the data in Craddock's work, we applied the %Ro vs H/C equation (10) to obtain a cross-plot of %Ro vs T. This shows that vitrinite reflectance (%Ro) exponentially increases with increase in simulation temperature (Fig. 7). This is expressed in equation (11).

$$T = 744.53\ln(\%Ro) + 2032.7 \quad (11)$$

which has a near-perfect coefficient of 0.95.

For Type III kerogen, there are significant differences in %Ro values calculated using the different equations (Fig. 8, lines a and d). Unlike the other formulas, the O/C atomic ratio was incorporated in equation (7) by Burnham and Sweeney (1989), resulting in much higher %Ro values. This discrepancy may be caused by the relatively small number of oxygen atoms in the kerogen molecular models used in this study.

The maturity levels in the temperature range 2200 K to 2600 K obtained using equation (4) are apparently underestimated. For example, the low H/C atomic ratio (< 0.4) at 2600 K suggests that kerogen degradation may have reached the late catagenesis stage (Fig. 6), corresponding to a vitrinite reflectance of about 2.0 %Ro. However, the value calculated by equation (4) is only 1.5 %Ro.

As mentioned, equations (5) and (6) are obtained from the same data

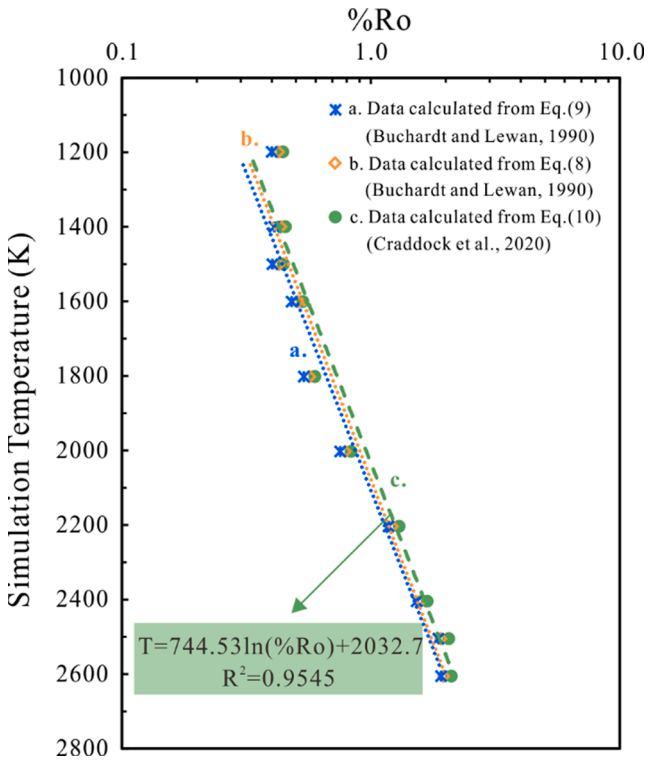

Fig. 7. Fitting formulas of molecular simulation temperatures and vitrinite reflectance for Type II kerogen, based on equations (8)–(10).

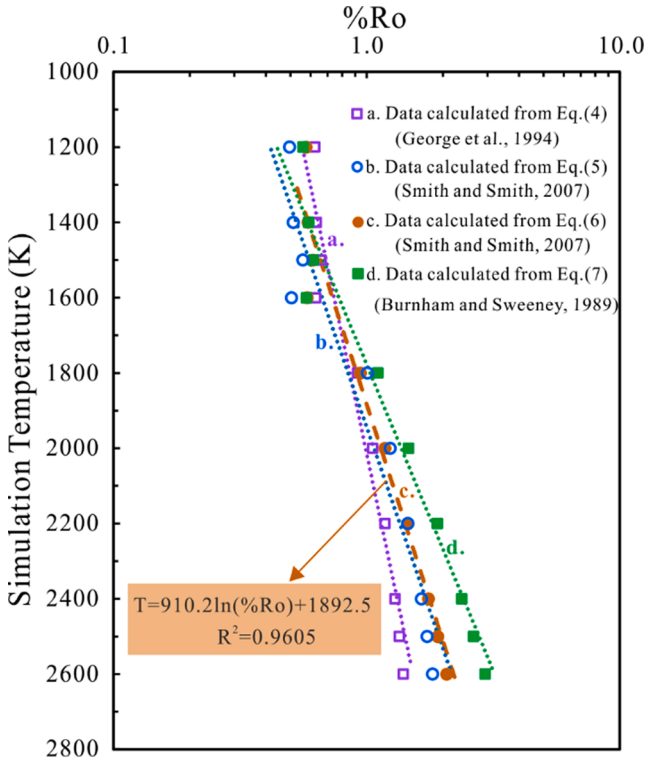

Fig. 8. Fitting formulas of molecular simulation temperature and vitrinite reflectance for Type III kerogen, based on equations (4)–(7).

set, with linear and exponential fits, respectively. Considering the exponential relationship of %Ro with burial depth i.e. temperature in the natural evolution process, equation (6) was selected in this study to calculate the equivalent %Ro values. Accordingly, the T (K) vs %Ro relationship for Type III kerogen was obtained as follows:

$$T = 910.2\ln(\%Ro) + 1892.5 \quad (12)$$

This equation has a high correlation coefficient ($r^2 = 0.96$).

As shown in Table 1, this study provides a practical and reliable maturity scale for the thermal degradation of Type II and III kerogen that links ReaxFF MD simulations with geological conditions. The simulation temperature of 1500 K is the onset of the oil generation window, corresponding to a vitrinite reflectance of approximately 0.5 %Ro for Type II kerogen, and 0.65 %Ro for Type III kerogen (Table 1). This indicates that oil generation from Type II kerogen occurs at an earlier stage of the maturation process than from Type III kerogen. This is a consequence of the comparatively high abundance of weaker bonds, such as the heteroatomic bonds that occur frequently in Type II kerogen (Kelemen et al., 2007). In addition, both the laboratory pyrolysis experiments (Pepper and Corvit, 1995; Behar et al., 1997) and ReaxFF MD simulation in this study show that the apparent activation energy for oil generation of Type II kerogen is lower than that of Type III kerogen (Fig. 5).

The simulation temperature of 2500–2600 K in this scale corresponds to a vitrinite reflectance of ~2.0 %Ro for both Type II and II kerogens (Table 1), indicating that thermal evolution of organic matter reaches the end of the catagenetic stage. Meanwhile, the H/C and O/C atomic ratios for the three types of kerogen are approximately the same at 2600 K (Figs. 3 and 4), because the similarities in the chemical compositions of kerogens become stronger at this stage (Vandenbroucke and Largeau, 2007).

The molecular simulation maturation trends are consistent with the thermal degradation processes of typical Type II and III kerogen in both laboratory experiments (Lewan, 1993) and under geological conditions (Craddock et al., 2018). Previous studies have also found that the temperature at the beginning of hydrocarbon generation for kerogen pyrolysis is approximately 1300 K on the MD time scale (Liu et al., 2015; Pawar et al., 2017), which corresponds to the equivalent vitrinite reflectance value of about 0.4–0.5 %Ro in this study. The maximum pyrolysis simulation temperature applied in previous ReaxFF MD simulations for kerogen pyrolysis is 2800 K, corresponding to a vitrinite reflectance of about 2.7 %Ro (extrapolated from the simulation maturity scale set out in this study), indicating that organic matter thermal evolution enters the metagenesis stage. The maturation scale established in this study is therefore reasonable and has sound practical implications for research on the thermal evolution of kerogen using ReaxFF MD simulation.

5. Conclusions

By comparing the relationships between measured vitrinite reflectance values and the H/C atomic ratios of kerogen reported in the literature, this preliminary study establishes a practical maturity scale of ReaxFF MD simulations for molecular modeling of the thermal degradation of kerogen. A large-scale reactive system with molecular models of three types of immature kerogen (types I, II and III) was used to simulate pyrolysis of kerogen at a range of temperatures, from 1200 K to 2600 K, using ReaxFF molecular dynamics. The H/C and O/C atomic ratios of residual kerogen fragments were determined at different

Table 1
Correspondence of molecular simulation temperatures of Type II and III kerogen to values for vitrinite reflectance (%Ro).

T_{MD} (K)	1200	1300	1400	1500	1600	1700	1800	1900
%Ro – II	0.33	0.37	0.43	0.49	0.56	0.64	0.73	0.84
%Ro – III	0.47	0.52	0.58	0.65	0.73	0.81	0.90	1.01
T_{MD} (K)	2000	2100	2200	2300	2400	2500	2600	2700
%Ro – II	0.96	1.09	1.25	1.43	1.64	1.87	2.14	2.45
%Ro – III	1.13	1.26	1.40	1.56	1.75	1.95	2.18	2.43

simulation temperatures which indicated that the H/C and O/C atomic ratios of kerogen molecules decreased with the increase of simulation temperature. The evolution of H/C vs O/C ratios of the three kerogen types modeled with MD simulations follows the same thermal maturation paths of geological kerogens demonstrated by the van Krevelen diagram. According to the first-order reaction kinetic model, the rate of reaction conforms to the Arrhenius equation. The corrected activation energy (*Ea*) for kerogen of the three types was calculated as 61.1 kcal/mol, 53.5 kcal/mol, and 52.8 kcal/mol, respectively, which is basically consistent with values obtained from both laboratory simulations and basin modeling. Based on the quantitative relationship between measured vitrinite reflectance (%Ro) and H/C atomic ratios in natural samples, logarithmic equations correlating %Ro with molecular simulation temperatures (T) of Type II and III kerogen are established using the H/C atomic ratios of kerogen as the link. This study provides practical and reasonable insights that will support extrapolation from molecular dynamics simulation temperatures to the actual geological evolution stages of kerogen.

Declaration of Competing Interest

The authors declare that they have no known competing financial interests or personal relationships that could have appeared to influence the work reported in this paper.

Data availability

The data that has been used is confidential.

Acknowledgements

This work was funded by the National Natural Science Foundation of China (Grant No. 42173054), the National Key R & D Program of China (Grant No. 2017YFC0603102), and the Natural Science Foundation of Sichuan Province (No. 2022NSFSC0182). All calculated results were provided by Sichuan University of Science & Engineering High Performance Computing Center. The authors would like to extend their appreciations to Dr. John K. Volkman (Co-Editor-in-Chief), Dr. J A Curiale (Associate Editor), Dr. Adri van Duin and an anonymous reviewer for their constructive comments and suggestions which significantly improved the quality of the manuscript. The authors also thank Dr. Xianggui Xue and Yushi Wen from the Institute of Chemical Materials, China Academy of Engineering Physics (CAEP) for their help with the LAMMPS code.

References

Accelrys. Materials-Studio. Available from the Internet at http://accelrys.com/products/materials-studio/, accessed October 11, 2013.
Aktulga, H.M., Fogarty, J.C., Pandit, S.A., Grama, A.Y., 2012. Parallel reactive molecular dynamics: Numerical methods and algorithmic techniques. Parallel Computing 38, 245–259.
Alpern, B., 1980. Petrographie du kerogene. In: Durand, B. (Ed.), Kerogen, Insoluble Organic Matter From Sedimentary Rocks. Technip Editions, Paris, France, pp. 339–384.
Atmani, L., Bichara, C., Pellenq, R.J.M., van Damme, H., van Duin, A.C.T., Raza, Z., Truflandier, L.A., Obliger, A., Kralert, P.G., Ulm, F.J., Leyssale, J., 2017. From cellulose to kerogen: Molecular simulation of a geological process. Chemical Science 8, 8325–8335.
Atmani, L., Valdenaire, P., Pellenq, R.J.M., Bichara, C., van Damme, H., van Duin, A.C.T., Ulm, F.J., Leyssale, J., 2020. Simulating the geological fate of terrestrial organic matter: Lignin vs cellulose. Energy & Fuels 34, 1537–1547.
Bandopadhyay, A.K., Mohanty, D., 2014. Variation in hydrogen content of vitrinite concentrates with rank advance. Fuel 134, 220–225.
Baskin, D.K., 1997. Atomic H/C ratio of kerogen as an estimate of thermal maturity and organic matter conversion. American Association of Petroleum Geologists Bulletin 81, 1437–1450.
Behar, F., Vandenbroucke, M., Tang, Y., Marquis, F., Espitalie, J., 1997. Thermal cracking of kerogen in open and closed systems; Determination of kinetic parameters and stoichiometric coefficients for oil and gas generation. Organic Geochemistry 26, 321–339.
Buchardt, B., Lewan, M.D., 1990. Reflectance of vitrinite-like macerals as a thermal maturity index for Cambrian-Ordovician alum shale, southern Scandinavia. American Association of Petroleum Geologists Bulletin 74, 394–406.
Burnham, A.K., 2015. A simple kinetic model of oil generation, vaporization, coking, and cracking. Energy & Fuels 29, 7156–7167.
Burnham, A.K., 2019. Kinetic models of vitrinite, kerogen, and bitumen reflectance. Organic Geochemistry 131, 50–59.
Burnham, A.K., Happe, J.A., 1984. On the mechanism of kerogen pyrolysis. Fuel 63, 1353–1356.
Burnham, A.K., Sweeney, J.J., 1989. A chemical kinetic model of vitrinite maturation and reflectance. Geochimica Geochimica et Cosmochimica Acta 53, 2649–2657.
Castro-Marcano, F., van Duin, A.C.T., 2013. Comparison of thermal and catalytic cracking of 1-heptene from ReaxFF reactive molecular dynamics simulations. Combustion and Flame 160, 766–775.
Chenoweth, K., van Duin, A.C.T., Goddard, W.A., 2008. ReaxFF reactive force field for molecular dynamics simulations of hydrocarbon oxidation. The Journal of Physical Chemistry A 112, 1040–1053.
Craddock, P.R., Haecker, A., Bake, K.D., Pomerantz, A.E., 2020. Universal curves describing the chemical and physical evolution of type II kerogen during thermal maturation. Energy & Fuels 34, 15217–15233.
Durand, B., 1980. Sedimentary organic matter and kerogen. Definition and quantitative importance. In: Kerogen, Editions Technip, Paris, pp. 13–34.
Fletcher, T.H., Kerstein, A.R., Pugmire, R.J., Solum, M.S., Grant, D.M., 1992. Chemical percolation model for devolatilization. 3. Direct use of carbon-13 NMR data to predict effects of coal type. Energy & Fuels 6, 414–431.
George, S.C., Smith, J.W., Jardine, D.R., 1994. Vitrinite reflectance suppression in coal due to a marine transgression: Case study of the organic geochemistry of the Greta seam, Sydney Basin. The APPEA Journal 34, 241–255.
Hong, D., Guo, X., 2017. Molecular dynamics simulations of Zhundong coal pyrolysis using reactive force field. Fuel 210, 58–66.
Huang, L., Ning, Z., Wang, Q., Zhang, W., Cheng, Z., Wu, X., Qin, H., 2018. Effect of organic type and moisture on CO_2/CH_4 competitive adsorption in kerogen with implications for CO_2 sequestration and enhanced CH_4 recovery. Applied Energy 210, 28–43.
Hunt, J.M., 1996. Petroleum Geochemistry and Geology, 2nd ed. W.H. Freeman, New York.
Kelemen, S.R., Afeworki, M., Gorbaty, M.L., Sansone, M., Kwiatek, P.J., Walters, C.C., Freund, H., Siskin, M., Bence, A.E., Curry, D.J., Solum, M., Pugmire, R.J., Vandenbroucke, M., Leblond, M., Behar, F., 2007. Direct characterization of kerogen by X-ray and solid-state ^{13}C nuclear magnetic resonance methods. Energy & Fuels 21, 1548–1561.
Leach, A., 2021. Molecular Modelling – Principles and Application, 2nd ed. World Book Press.
Lewan, M.D., 1987. Petrographic study of primary petroleum migration in the Woodford Shale and related rock units. Collection colloques et séminaires-Institut français du pétrole 113–130.
Lewan, M.D., 1993. Identifying and understanding suppressed vitrinite reflectance through hydrous pyrolysis experiments. 10th Annual Meeting, Abstracts and Program. The Society for Organic Petrology.
Li, M., Liu, X., Han, Q., Xiao, H., Fang, R., He, D., Gao, Z., 2021. Progress of molecular simulation application research in petroleum geochemistry. Oil & Gas Geology 42, 919–930.
Liu, X., Zhan, J., Lai, D., Liu, X., Zhang, Z., Xu, G., 2015. Initial pyrolysis mechanism of oil shale kerogen with reactive molecular dynamics simulation. Energy & Fuels 29, 2987–2997.
Liu, X., Li, M., Zhang, C., Fang, R., Zhong, N., Xue, Y., Zhou, Y., Jiang, W., Chen, X., 2020. Mechanistic insight into the optimal recovery efficiency of CBM in sub-bituminous coal through molecular simulation. Fuel 266, 117137.
Lohr, C.D., Hackley, P.C., 2021. Relating Tmax and hydrogen index to vitrinite and solid bitumen reflectance in hydrous pyrolysis residues: Comparisons to natural thermal indices. International Journal of Coal Geology 242, 103768.
Paajanen, A., Vaari, J., 2017. High-temperature decomposition of the cellulose molecule: A stochastic molecular dynamics study. Cellulose 24, 2713–2725.
Pawar, G., Meakin, P., Huang, H., 2017. Reactive molecular dynamics simulation of kerogen thermal maturation and cross-linking pathways. Energy & Fuels 31, 11601–11614.
Pepper, A.S., Corvit, P.J., 1995. Simple kinetic models of petroleum formation; Part I, Oil and gas generation from kerogen. Marine and Petroleum Geology 12, 291–319.
Qian, Y., Zhan, J., Lai, D., Li, M., Liu, X., Xu, G., 2016. Primary understanding of non-isothermal pyrolysis behavior for oil shale kerogen using reactive molecular dynamics simulation. International Journal of Hydrogen Energy 41, 12093–12100.
Salmon, E., van Duin, A.C.T., Lorant, F., Marquaire, P., Goddard, W.A., 2009. Early maturation processes in coal. Part 2: Reactive dynamics simulations using the ReaxFF reactive force field on Morwell brown coal structures. Organic Geochemistry 40, 1195–1209.
Seyyedattar, M., Zendehboudi, S., Butt, S., 2019. Molecular dynamics simulations in reservoir analysis of offshore petroleum reserves: A systematic review of theory and applications. Earth-Science Reviews 192, 194–213.
Shinoda, W., Shiga, M., Mikami, M., 2004. Rapid estimation of elastic constants by molecular dynamics simulation under constant stress. Physical Review B 69, 134103.
Sinninghe Damsté, J.S., Eglinton, T.I., de Leeuw, J.W., Schenck, P.A., 1989. Organic sulphur in macromolecular sedimentary organic matter; I, Structure and origin of sulphur-containing moieties in kerogen, asphaltenes and coal as revealed by flash pyrolysis. Geochimica et Cosmochimica Acta 53, 873–889.

Smith, J.R., Smith, J.W., 2007. A relationship between the carbon and hydrogen content of coals and their vitrinite reflectance. International Journal of Coal Geology 70, 79–86.
So Rensen, M.R., Voter, A.F., 2000. Temperature-accelerated dynamics for simulation of infrequent events. The Journal of Chemical Physics 112, 9599–9606.
Sweeney, J., Burnham, A.K., 1990. Evaluation of a simple model of vitrinite reflectance based on chemical kinetics. American Association of Petroleum Geologists Bulletin 74, 1559–1570.
Tang, Y., Jenden, P.D., Nigrini, A., Teerman, S.C., 1996. Modeling early methane generation in coal. Energy & Fuels 10, 659–671.
Tissot, P.B., Welte, D.H., 1984. Petroleum Formation and Occurrence. Springer.
Ungerer, P., Durand, B., Behar, F., 1990. State of the art of research in kinetic modelling of oil formation and expulsion. Organic Geochemistry 16, 1–25.
Ungerer, P., Collell, J., Yiannourakou, M., 2015. Molecular modeling of the volumetric and thermodynamic properties of kerogen: Influence of organic type and maturity. Energy & Fuels 29, 91–105.
Valdenaire, P., Pellenq, R.J.M., Ulm, F.J., van Duin, A.C.T., Leyssale, J., 2020. Timescale prediction of complex multi-barrier pathways using flux sampling molecular dynamics and 1D kinetic integration: Application to cellulose dehydration. The Journal of Chemical Physics 152, 24123.
van Duin, A.C.T., Dasgupta, S., Lorant, F., Goddard, W.A., 2001. ReaxFF: A reactive force field for hydrocarbons. The Journal of Physical Chemistry A 105, 9396–9409.
van Krevelen, D.W., 1961. Coal: Typology - Chemistry - Physics - Constitution, pp. 238–262.
Vandenbroucke, M., Largeau, C., 2007. Kerogen origin, evolution and structure. Organic Geochemistry 38, 719–833.
Wang, S., Feng, Q., Zha, M., Javadpour, F., Hu, Q., 2018. Supercritical methane diffusion in shale nanopores: Effects of pressure, mineral types, and moisture content. Energy & Fuels 32, 169–180.
Xu, F., Liu, H., Wang, Q., Pan, S., Zhao, D., Liu, Q., Liu, Y., 2019. ReaxFF-based molecular dynamics simulation of the initial pyrolysis mechanism of lignite. Fuel Processing Technology 195, 106147.
Xue, X., Meng, L., Ma, Y., Zhang, C., 2017. Molecular Reactive Force-Field simulations on the carbon nanocavities from methane pyrolysis. The Journal of Physical Chemistry C 121, 7502–7513.
Yang, Y., Liu, J., Yao, J., Kou, J., Li, Z., Wu, T., Zhang, K., Zhang, L., Sun, H., 2020. Adsorption behaviors of shale oil in kerogen slit by molecular simulation. Chemical Engineering Journal 387, 124054.
Zhang, Z., Guo, L., Zhang, H., 2021. A ReaxFF molecular dynamics study on the hydropyrolysis process of Huadian oil shale kerogen. Molecular Simulation 47, 334–345.
Zhang, L., LeBoeuf, E.J., 2009. A molecular dynamics study of natural organic matter: 1. Lignin, kerogen and soot. Organic Geochemistry 40, 1132–1142.
Zhang, X., Lu, X., Xiao, M., Lin, R., Zhou, Z., 2020. Molecular reaction dynamics simulation of pyrolysis mechanism of typical bituminous coal via ReaxFF. Journal of Fuel Chemistry and Technology 48, 1035–1046.
Zheng, M., Li, X., Liu, J., Wang, Z., Gong, X., Guo, L., Song, W., 2014. Pyrolysis of liulin coal simulated by GPU-Based ReaxFF MD with cheminformatics analysis. Energy & Fuels 28, 522–534.